united nations
educational, scientific
and cultural
organization

international atomic
energy agency

the
abdus salam
international centre for theoretical physics

SMR/1328/20

School on the Physics of Equatorial Atmosphere

(24 September - 5 October 2001)

Synthesis: Examples of Ionospheric Disturbances Revealed by Radio Diagnostics

M. A. Abdu
(Instituto Nacional de Pesquisas Espaciais, São José dos Campos, Brazil)

Synthesis: Examples of ionospheric disturbances revealed by radio diagnostics.

Ionospheric disturbances originate from (1)- Solar disturbances and (2)- Neutral atmospheric disturbance associated with (1) and due to forcing from middle and lower atmosphere.

Ionospheric disturbances of solar activity origin have been investigated extensively using ground based radio diagnostics during the last 4-5 decades and a synthetic knowledge of the cause- effect relationship is now available. On the other hand the ioniospheric response signatures of disturbances originating from lower regions of the atmosphere is poorly understood.

The ionospheric disturbances having genesis in solar disturbances can be broadly classified into two types:

1- Those produced by the effect of electromagnetic radiation emitted by solar flares (X-rays and EUV);

2- Disturbances that follow within few minutes to hours and to few days from the onset of a flare. Energetic and relativistic particles and Coronal Mass Ejection –CME (from solar flares and active regions on the sun) that hit the earth's magnetosphere and atmosphere, cause these.

The sequences of 1 and 2 are represented in **Fig.1**.

Sudden ionospheric disturbances:

These are short-lived events that occur in the various ionospheric layers, but are most pronounced in the D layer. An example of a flare associated sudden increases in the X-rays of wavelength ranges 1- 8 A 0.5 – 3.5 A are shown in **Fig.2**. Increase in electron density in the lower ionosphere produced by such enhanced x-ray fluxes is shown in **Fig. 3.**

A list of well-known events of sudden ionospheric disturbances is given in the following table

Table: Types of Sudden Ionospheric Disturbances- SID

Name and nomenclature	**Primary layer**	**Effect**
Short wave fade out (SWF)	D	HF amplitude
Sudden phase anomaly (SPA)	D	Very Low Frequency (VLF phase
Sudden enhancement of signal (SES)	D	VLF amplitude
Sudden enhancement of atmospherics (SEA)	D	LF/VLH noise
Sudden cosmic noise absorption (SCNA)	D	HF and lower VHF
Increase of foE	E	HF
Increase of foF2	F2	HF
Sudden increase in total electron content (SITEC)	E – F	HF- VHF frequency and phase

Some examples of these effects are presented in the following figures.

Fig.4a- Effect of short X-rays on the day side at frequencies 5,10 and 20 MHz (McNamara, 1991),

Figs. 4b shows an example of one of the earliest detection of SWF at 9.570 MHz and a simultaneous effect on the geomagnetic field (crochet).

Fig. 5 shows the SWF effect as recorded by a sweep frequency HF sounder together with the associated flare X-ray intensity variation.

Fig.6- shows an example of an SPA observed at 9.34 kHz plotted with the corresponding X-ray flux. The sudden change in the VLF phase is due to the lowering of the D region reflection height as the relationship:

$$\Delta h = \lambda \, \Delta\phi (d^2 + h^2)^{1/2} / 4\pi h.$$

Where λ is the wavelength of the VLF wave, 2d is the ground distance, and h is the height of the equivalent mirror reflection.

An example of a sudden cosmic noise absorption event at 10 MHz in the ordinary and extra ordinary waves is shown in **Fig 7**

The sudden changes in the D region associated with solar X-rays can be used to investigate the complex chemistry of this region. The early results have been used for investigating the recombination processes determined by simple molecular chemistry of the D region. However, many complexities of the D region chemistry have been revealed in recent years.

Fig.8 shows an example of sudden increase in total electron content. Such information can be used to infer the enhancement in solar EUV that can occur during solar flares.

Delayed Effects:

The delayed effects can occur within a few minutes to a few hours to several days from the initiation of a solar disturbance. They arise from energetic particles and CME's associated with the flares that hit the earth with varying time delays. An example of effects from energetic particle is known as Polar Cap Absorption event (PCA) when HF and VHF absorption and radio black out occurs in polar regions that can last several days. A PCA is caused by high –energy protons from large flares which penetrate to lower altitude of the atmosphere which causes large increases in the electron density in the polar D region. This increase in density leads to large increase in HF/VHF absorption that can last for several days depending upon the output of protons from the flare. There is usually some recovery of the signal strength during hours of darkness. This is illustrated in **Fig.9**

The CME and high speed solar wind that hit the magnetosphere produce disturbances observed as magnetic storms all over the globe. During such disturbances magnetospheric energy is deposited at auroral latitudes in the form of particle precipitation and large-scale electric field that produce auroral substorms involving enhanced electrojet current and Joule heating of the auroral E region. The magnetospheric electric fields penetrate to equatorial latitude where prompt response features are observed. The heating of the auroral thermosphere produces thermospheric disturbances in the form of upwelling, and equator-ward propagating disturbance winds and gravity waves which produce delayed effects over middle low and equatorial latitudes. The thermospheric composition is altered with increased ratio of $[N_2]/[O]$ that causes decrease in F region electron density in a wide range of latitude extending equator-ward during major storms. Equatorward meridional wind could rise the F layer heights to cause increase of electron density.

The observed ionospheric effects differ with latitude

***High Latitude effects*:** Ionospheric effects observed over high latitude are highly complex. The most common effects observed by radio techniques concern (1) ionization produce by particle precipitation seen as additional/enhanced layers in the ionograms (2)-changes in plasma convection pattern drive by magnetospheric electric fields, as observed by HF and VHF radars, and digital ionosonds.

Effects over Middle latitudes

D- region effects: The D region over mid-latitude experience changes of longer duration. An example of such effect observed by LF/VLF techniques is presented in **Fig.10.** The reflection height of the 16 kHz radio wave is lowered as seen in the phase advance indicating enhanced electron density around 70-80 km. Such effect is called storm after effect, as it tends to follow a magnetic storm. During this event the absorption of the VLF waves is increased. The effect continues for several days after magnetic elements have returned to normal. There are two hypothesis suggested to explain the effect:

1- Electron precipitation from outer radiation belt. The existence of precipitation over mid-latitude has been revealed by satellite data. Refilling of plasmasphere with cold plasma has been suggested as a possible cause of this precipitation, but quantitative verification is lacking.
2- Particle precipitation at high latitude produce nitric oxide which could be transported to middle latitude where solar Layman -α radiation could enhance electron production.

F region effects:

The F layer peak density foF2 and height hmF2 and total electron content (TEC) of the ionosphere can be drastically modified during the course of a magnetic disturbance. The foF2 increase (decrease) with respect to its quiet time value is known as positive (negative) phase of an ionospheric storm. Negative phase of the ionospheric storm is more common during the main and recovery phases of a magnetic storm disturbance. Positive phase of the ionospheric disturbance is observed mostly in the early phase of the magnetic disturbance. Such effects are season and local time dependent.

Fig.11 shows storm time variation of the maximum electron density (N_mF2) deviation from quiet day average value, as obtained from ionosonde observations, for a wide range of geomagnetic latitudes. The storm effect is greatest at middle latitudes extending to higher latitudes as well. The figure shows also that the effect is weaker for weak storms. Over low latitude the effect tends to be more of a positive phase.

The effects on N_mF2 and TEC for a specific storm are shown in **Fig.12**.

Some results from a global analysis of F region storm effects is presented in **Fig. 13**. The results diurnal characteristics of foF2 over a few mid-latitude stations during a disturbance interval, in September 1989 when three magnetic storms occurred, are shown in this figure.

Some recent results of response features to storms of moderate intensity in the Southern Hemisphere are shown in **Fig. 14**. The responses are shown for middle and low latitude stations in American longitude sector (from Xemena et al JGR submitted, 2001). These results show, for mid latitude station King George Island, strong negative phase presumably produced by disturbance in thermospheric composition (that is, increased ratio of $[N_2]/[O]$, that lasted several days after the storm.

Disturbance effects over equatorial latitudes:

Magnetic storm associated ionospheric disturbances effects over low and equatorial latitudes are rather complex due to the fact that such effects arise from: (a) disturbance magnetospheric electric fields that penetrate to equatorial latitude promptly with the rapid changes in auroral activity (the growth, development and decay phases of a substorm), (b) delayed effects resulting from the thermospheric disturbance that propagate

equatorward from the source of energy deposition at auroral latitudes. Equatorial ionospheric responses arises due to the disturbance dynamo electric field and disturbance thermospheric winds (meridional and zonal components), and (c) superimposed effects arising from both (a) and (b) during magnetospheric disturbance of extended duration.

All the major equatorial phenomena suffer significant modification during such disturbances. Depending upon the disturbance phase of the storm: The equatorial ionosphere can undergo large increase or decrease in height; the anomaly could be enhanced, the subtropical ionization peaks extending poleward; the anomaly formation can be inhibited more often, however; equatorial plasma instability process of the E and F regions can be inhibited or enhanced; equatorial electrojet intensity can be enhanced, inhibited or reversed. .

An example of disturbance induced vertical plasma drift during post midnight hours observed by Jicamarca Radar is shown in **Fig.15**. This large increase of the vertical drift can trigger spread F instabilities (not shown here). Another case of F layer uplift observed over Brazil which is produced by a disturbance eastward electric field (prompt penetration electric field) associated with a magnetic storm is presented in **Fig. 16**. Such disturbance electric field has opposing polarity in opposite hemisphere, as shown in **Fig.17**. Consequently the ionospheric density perturbations have opposite phases in locations widely separated in longitude.

A disturbance electric field can modify the equatorial anomaly. An eastward electric field can cause enhancement of the anomaly and a westward electric field can cause its inhibition. Some cases of such response features are shown in **Fig.14**. An example of the anomaly expansion as seen in the TEC variation over Cachoeira Paulista is presented in **Fig.18**.

For intense storms such as that occurred during March 1989, the disturbance electric field has large magnitude that could cause large uplift of the F layer. During the March 1989 storm large eastward electric field caused the uplift of the F layer to heights above 1000km, the usual range limit of the ionosondes, Such large electric field caused the 'disappearance' of ionospheric in the ionogram over the equatorial and low latitude sites in Brazil, indicating poleward expansion of the anomaly to such a degree that the TEC over C. Paulista showed severe depletion. Concurrent increase in the TEC was observed at higher latitude poleward into the mid-latitude as shown in the results of **Figs.19 and 20**.

The global responses of the ionosphere in terms of the deviation from quiet conditions of the F2 layer peak density (foF2) are presented in **Figs. 21** for the great storm of October 1989.

Ionospheric disturbance can manifest as modification of the instability processes arising from the imposed disturbance electric field. An eastward (westward) disturbance electric field can cause enhancement (inhibition) of instabilities in the electrojet as well as in the F region. Some examples of changes taking place in the electrojet instability processes

are presented in **Figs. 22 a,b and 23**. An example of enhanced plasma bubble structures due to a disturbance eastward electric field that occurred superimposed on the normal evening prereversal electric field is shown in **Fig.24**.

Fig.1- The events in interplanetary space that follow a large solar flare: (1) Top- X-rays are one form of radiation emitted by the flare. These travel in straight lines at the velocity of light, taking about 8 minutes to reach the earth; (2) Middle- Fast protons reach the earth after a delay which can be as short as a few minutes. These are followed by the more slowly moving flare cloud, which is preceded by a shock at the position where the clouds hit the quiet solar wind; (3) Lower- The flare could reaches the earth a few days after being ejected from the flare.

Fig.2- Sample X-ray flare showing sudden increase in the 1-8A and .5- 3.6 A channels. The hardness ratio (0.5-3.6A flux)/1.8A flux) increases near the peak.

Fig.3- The computed increase of electron density due to flux increases in the stated wave length intervals (from A. D. Richmond, quoted by Hargreaves, (Solar- Terrestrial environment, Cambridge press, 1992)

Fig.4- A short wave fadeout and a magnetic crochet (sudden flare effect) on November 1936).

Fig.5- HF sounder data plot of an SWF variation with time of the radio frequencies observed on 30th October 1968 over the 4000 km path Hawaii to Corona, California during an X-ray burst (Bleiwiess et al., Tech, Report TR 1868, Naval Electronics Lab Center, San Diego, California, 1973).

Fig.6- A comparison of the 9.34 kHz phase and X-ray flux (inner scale, in ergs cm^{-2} s^{-1}) during a sudden phase anomaly on July 1968(Bleiweiss at al., 1973).

Fig.7- Sudden Cosmic noise absorption, 10 MHz at Collage, Alaska
on June 11, 1961(Lawrence et al., Proc. IEEE, 52:4-27, 1964).

Fig.8- Sudden increase in total electron content, ATS- Boulder, July 4, 1074.

Fig.9-An illustration of a Polar Cap absorption event (McNamara, The Ionosphere, Communication, Surveillance and direction finding, Kreiger Publishing Company, Florida, 1991).

Fig.10- A D region storm as seen in VLF radio propagation: reflection height of 16 kHz waves over the path Rugby- Cambridge, UK, during a magnetic storm in 1956(J. S. Belrose AGARD Report 29, 1968, as quoted by Hargreaves, 1991).

Fig.11- Storm time variation of maximum electron density (N_mF2), in eight zones of geomagnetic latitude. The ordinate is the percentage deviation from quiet-day behavior (S. Matsushita, JGR, 64, 305, 1959).

Fig.12- Electron content, electron density and slab thickness at a mid-latitude station during an F region storm. SC marks the time of the sudden commencement. The 7-day means is also shown to indicate the normal behavior (Mendillo and Klobuchar, Report AFGRL-TR-74-0065, US Air Force, 1974).

Fig. 13- Diurnal characteristics of the F region density for the period September 14-29 1989, as measured by the critical frequency foF2 (=8.9 (10) ^{3} $N_mF2^{1/2}$ -(N_mF2 being in cm^{-3})- in a chain of northern midlatitude to high latitude stations. (Szuszczewicz et al., JGR, 103, 11,665-11,684, 1998).

Fig.14- The Auroral Activity index AE, the 3-hourly Planetary index K_p and the D_{st} values during 20-24 October 1989 corresponding the magnetic storm disturbance that had onset at ~08 UT on 20 October, plotted in the first top three panels. The two bottom panels show the variations of f_oF_2 and h_mF_2 during these days for the four locations Fortaleza (FZ), Cachoeira Paulista (CP), Concepción (CON) and King George Island (KGI). Horizontal patches indicate night hours for each of the stations. Horizontal lines with identification numbers, 1, 2, 3 etc. along the h_mF_2 plot over CP indicate intervals when positive and negative disturbances in meridional winds occurred.

Fig.15- Mass plot of vertical drift pattern over Jicamarca radar. The large increase of the vertical drift on one of the nights is due to a disturbance eastward electric field.

Fig.16- Variation pattern in response to the magnetic storm of 24-25 March in panels top to bottom (a) F layer height and peak density over Fortaleza, (b) same parameters over Cachoeira Paulista, (c) H- component of magnetic field, and (d) asymmetric ring current index which is equivalent to auroral activity index.

Fig.17- Variations in F layer heights over Fortaleza in Brazil and Hong Kong (top and middle panels). The disturbance has opposite polarity at the two location during the morning hours whereas the same polarity prevails in the evening hours.

Fig.18- Total electron content variation over Cachoeira Paulista during March 24-25 storm suggests poleward expansion of the equatorial anomaly peaks.

Fig.19- The variations of the F region height and peak density over the Brazilian stations Fortaleza and Cachoeira Paulista (located at the anomaly trough and crest, respectively) showing the large uplift of the layer in the dusk sector (to higher than the 1000 km limit

of the ionosonde), causing large TEC depletion confirming the anomaly peak dislocation suggested from Figs. 18,19 and 20.

Fig.20- TEC variations over Cachoeira Paulista in Brazil and over some higher latitude locations in Northern hemisphere during the great magnetic storm of March 1989, suggesting poleward expansion of the equatorial anomaly.

Fig.21- Contours of foF2 deviation vs. latitude and time for the Asian –Pacific sector during October 20-22, 1989

Synthesis: Examples of ionospheric disturbances revealed by radio diagnostics.

Ionospheric disturbances originate from (1)- Solar disturbances and (2)- Neutral atmospheric disturbance associated with (1) and due to forcing from middle and lower atmosphere.

Ionospheric disturbances of solar activity origin have been investigated extensively using ground based radio diagnostics during the last 4-5 decades and a synthetic knowledge of the cause- effect relationship is now available. On the other hand the ioniospheric response signatures of disturbances originating from lower regions of the atmosphere is poorly under.

The ionospheric disturbances having genesis in solar disturbances can be broadly classified into two types:

1- Those produced by the effect of electromagnetic radiation emitted by solar flares (X-rays and EUV);

2- Disturbances that follow within few minutes to hours and to few days from the onset of a flare. Energetic and relativistic particles and Coronal Mass Ejection –CME (from solar flares and active regions on the sun) that hit the earth's magnetosphere and atmosphere, cause these.

The sequences of 1 and 2 are represented in **Fig.1**.

Sudden ionospheric disturbances:

These are short-lived events that occur in the various ionospheric layers, but are most pronounced in the D layer. An example of a flare associated sudden increases in the X-rays of wavelength ranges 1- 8 A 0.5 – 3.5 A are shown in **Fig.2**. Increase in electron density in the lower ionosphere produced by such enhanced x-ray fluxes is shown in **Fig. 3.**

A list of well-known events of sudden ionospheric disturbances is given in the following table

Table: Types of Sudden Ionospheric Disturbances- SID

Name and nomenclature	**Primary layer**	**Effect**
Short wave fade out (SWF)	D	HF amplitude
Sudden phase anomaly (SPA)	D	Very Low Frequency (VLF phase
Sudden enhancement of signal (SES)	D	VLF amplitude
Sudden enhancement of atmospherics (SEA)	D	LF/VLH noise
Sudden cosmic noise absorption (SCNA)	D	HF and lower VHF
Increase of foE	E	HF
Increase of foF2	F2	HF
Sudden increase in total electron content (SITEC)	E – F	HF- VHF frequency and phase

Some examples of these effects are presented in the following figures.

Fig.4a- Effect of short X-rays on the day side at frequencies 5,10 and 20 MHz (McNamara, 1991),

Figs. 4b shows an example of one of the earliest detection of SWF at 9.570 MHz and a simultaneous effect on the geomagnetic field (crochet).

Fig. 5 shows the SWF effect as recorded by a sweep frequency HF sounder together with the associated flare X-ray intensity variation.

Fig.6- shows an example of an SPA observed at 9.34 kHz plotted with the corresponding X-ray flux. The sudden change in the VLF phase is due to the lowering of the D region reflection height as the relationship:

$$\Delta h = \lambda \, \Delta\phi (d^2 + h^2)^{1/2} / 4\pi h.$$

Where λ is the wavelength of the VLF wave, 2d is the ground distance, and h is the height of the equivalent mirror reflection.

An example of a sudden cosmic noise absorption event at 10 MHz in the ordinary and extra ordinary waves is shown in **Fig 7**

The sudden changes in the D region associated with solar X-rays can be used to investigate the complex chemistry of this region. The early results have been used for investigating the recombination processes determined by simple molecular chemistry of the D region. However, many complexities of the D region chemistry have been revealed in recent years.

Fig.8 shows an example of sudden increase in total electron content. Such information can be used to infer the enhancement in solar EUV that can occur during solar flares.

Delayed Effects:

The delayed effects can occur within a few minutes to a few hours to several days from the initiation of a solar disturbance. They arise from energetic particles and CME's associated with the flares that hit the earth with varying time delays. An example of effects from energetic particle is known as Polar Cap Absorption event (PCA) when HF and VHF absorption and radio black out occurs in polar regions that can last several days. A PCA is caused by high –energy protons from large flares which penetrate to lower altitude of the atmosphere which causes large increases in the electron density in the polar D region. This increase in density leads to large increase in HF/VHF absorption that can last for several days depending upon the output of protons from the flare. There is usually some recovery of the signal strength during hours of darkness. This is illustrated in **Fig.9**

The CME and high speed solar wind that hit the magnetosphere produce disturbances observed as magnetic storms all over the globe. During such disturbances magnetospheric energy is deposited at auroral latitudes in the form of particle precipitation and large-scale electric field that produce auroral substorms involving enhanced electrojet current and Joule heating of the auroral E region. The magnetospheric electric fields penetrate to equatorial latitude where prompt response features are observed. The heating of the auroral thermosphere produces thermospheric disturbances in the form of upwelling, and equator-ward propagating disturbance winds and gravity waves which produce delayed effects over middle low and equatorial latitudes. The thermospheric composition is altered with increased ratio of $[N_2]/[O]$ that causes decrease in F region electron density in a wide range of latitude extending equator-ward during major storms. Equatorward meridional wind could rise the F layer heights to cause increase of electron density.

The observed ionospheric effects differ with latitude

High Latitude effects: Ionospheric effects observed over high latitude are highly complex. The most common effects observed by radio techniques concern (1) ionization produce by particle precipitation seen as additional/enhanced layers in the ionograms (2)-changes in plasma convection pattern drive by magnetospheric electric fields, as observed by HF and VHF radars, and digital ionosonds.

Effects over Middle latitudes

D- region effects: The D region over mid-latitude experience changes of longer duration. An example of such effect observed by LF/VLF techniques is presented in **Fig.10.** The reflection height of the 16 kHz radio wave is lowered as seen in the phase advance indicating enhanced electron density around 70-80 km. Such effect is called storm after effect, as it tends to follow a magnetic storm. During this event the absorption of the VLF waves is increased. The effect continues for several days after magnetic elements have returned to normal. There are two hypothesis suggested to explain the effect:

1- Electron precipitation from outer radiation belt. The existence of precipitation over mid-latitude has been revealed by satellite data. Refilling of plasmasphere with cold plasma has been suggested as a possible cause of this precipitation, but quantitative verification is lacking.
2- Particle precipitation at high latitude produce nitric oxide which could be transported to middle latitude where solar Layman -α radiation could enhance electron production.

F region effects:

The F layer peak density foF2 and height hmF2 and total electron content (TEC) of the ionosphere can be drastically modified during the course of a magnetic disturbance. The foF2 increase (decrease) with respect to its quiet time value is known as positive (negative) phase of an ionospheric storm. Negative phase of the ionospheric storm is more common during the main and recovery phases of a magnetic storm disturbance. Positive phase of the ionospheric disturbance is observed mostly in the early phase of the magnetic disturbance. Such effects are season and local time dependent.

Fig.11 shows storm time variation of the maximum electron density (N_mF2) deviation from quiet day average value, as obtained from ionosonde observations, for a wide range of geomagnetic latitudes. The storm effect is greatest at middle latitudes extending to higher latitudes as well. The figure shows also that the effect is weaker for weak storms. Over low latitude the effect tends to be more of a positive phase.

The effects on N_mF2 and TEC for a specific storm are shown in **Fig.12**.

Some results from a global analysis of F region storm effects is presented in **Fig. 13**. The results diurnal characteristics of foF2 over a few mid-latitude stations during a disturbance interval, in September 1989 when three magnetic storms occurred, are shown in this figure.

Some recent results of response features to storms of moderate intensity in the Southern Hemisphere are shown in **Fig. 14**. The responses are shown for middle and low latitude stations in American longitude sector (from Xemena et al JGR submitted, 2001). These results show, for mid latitude station King George Island, strong negative phase presumably produced by disturbance in thermospheric composition (that is, increased ratio of $[N_2]/[O]$, that lasted several days after the storm.

Disturbance effects over equatorial latitudes:

Magnetic storm associated ionospheric disturbances effects over low and equatorial latitudes are rather complex due to the fact that such effects arise from: (a) disturbance magnetospheric electric fields that penetrate to equatorial latitude promptly with the rapid changes in auroral activity (the growth, development and decay phases of a substorm), (b) delayed effects resulting from the thermospheric disturbance that propagate

equatorward from the source of energy deposition at auroral latitudes. Equatorial ionospheric responses arises due to the disturbance dynamo electric field and disturbance thermospheric winds (meridional and zonal components), and (c) superimposed effects arising from both (a) and (b) during magnetospheric disturbance of extended duration.

All the major equatorial phenomena suffer significant modification during such disturbances. Depending upon the disturbance phase of the storm: The equatorial ionosphere can undergo large increase or decrease in height; the anomaly could be enhanced, the subtropical ionization peaks extending poleward; the anomaly formation can be inhibited more often, however; equatorial plasma instability process of the E and F regions can be inhibited or enhanced; equatorial electrojet intensity can be enhanced, inhibited or reversed. .

An example of disturbance induced vertical plasma drift during post midnight hours observed by Jicamarca Radar is shown in **Fig.15**. This large increase of the vertical drift can trigger spread F instabilities (not shown here). Another case of F layer uplift observed over Brazil which is produced by a disturbance eastward electric field (prompt penetration electric field) associated with a magnetic storm is presented in **Fig. 16**. Such disturbance electric field has opposing polarity in opposite hemisphere, as shown in **Fig.17**. Consequently the ionospheric density perturbations have opposite phases in locations widely separated in longitude.

A disturbance electric field can modify the equatorial anomaly. An eastward electric field can cause enhancement of the anomaly and a westward electric field can cause its inhibition. Some cases of such response features are shown in **Fig.14**. An example of the anomaly expansion as seen in the TEC variation over Cachoeira Paulista is presented in **Fig.18**.

For intense storms such as that occurred during March 1989, the disturbance electric field has large magnitude that could cause large uplift of the F layer. During the March 1989 storm large eastward electric field caused the uplift of the F layer to heights above 1000km, the usual range limit of the ionosondes, Such large electric field caused the 'disappearance' of ionospheric in the ionogram over the equatorial and low latitude sites in Brazil, indicating poleward expansion of the anomaly to such a degree that the TEC over C. Paulista showed severe depletion. Concurrent increase in the TEC was observed at higher latitude poleward into the mid-latitude as shown in the results of **Figs.19 and 20**.

The global responses of the ionosphere in terms of the deviation from quiet conditions of the F2 layer peak density (foF2) are presented in **Figs. 21** for the great storm of October 1989.

Ionospheric disturbance can manifest as modification of the instability processes arising from the imposed disturbance electric field. An eastward (westward) disturbance electric field can cause enhancement (inhibition) of instabilities in the electrojet as well as in the F region. Some examples of changes taking place in the electrojet instability processes

are presented in **Figs. 22 a,b and 23**. An example of enhanced plasma bubble structures due to a disturbance eastward electric field that occurred superimposed on the normal evening prereversal electric field is shown in **Fig.24**.

Fig.1- The events in interplanetary space that follow a large solar flare: (1) Top- X-rays are one form of radiation emitted by the flare. These travel in straight lines at the velocity of light, taking about 8 minutes to reach the earth; (2) Middle- Fast protons reach the earth after a delay which can be as short as a few minutes. These are followed by the more slowly moving flare cloud, which is preceded by a shock at the position where the clouds hit the quiet solar wind; (3) Lower- The flare could reaches the earth a few days after being ejected from the flare.

Fig.2- Sample X-ray flare showing sudden increase in the 1-8A and .5- 3.6 A channels. The hardness ratio (0.5-3.6A flux)/1.8A flux) increases near the peak.

Fig.3- The computed increase of electron density due to flux increases in the stated wave length intervals (from A. D. Richmond, quoted by Hargreaves, (Solar- Terrestrial environment, Cambridge press, 1992)

Fig.4- A short wave fadeout and a magnetic crochet (sudden flare effect) on November 1936).

Fig.5- HF sounder data plot of an SWF variation with time of the radio frequencies observed on 30th October 1968 over the 4000 km path Hawaii to Corona, California during an X-ray burst (Bleiwiess et al., Tech, Report TR 1868, Naval Electronics Lab Center, San Diego, California, 1973).

Fig.6- A comparison of the 9.34 kHz phase and X-ray flux (inner scale, in ergs cm^{-2} s^{-1}) during a sudden phase anomaly on July 1968(Bleiweiss at al., 1973).

Fig.7- Sudden Cosmic noise absorption, 10 MHz at Collage, Alaska
on June 11, 1961(Lawrence et al., Proc. IEEE, 52:4-27, 1964).

Fig.8- Sudden increase in total electron content, ATS- Boulder, July 4, 1074.

Fig.9-An illustration of a Polar Cap absorption event (McNamara, The Ionosphere, Communication, Surveillance and direction finding, Kreiger Publishing Company, Florida, 1991).

Fig.10- A D region storm as seen in VLF radio propagation: reflection height of 16 kHz waves over the path Rugby- Cambridge, UK, during a magnetic storm in 1956(J. S. Belrose AGARD Report 29, 1968, as quoted by Hargreaves, 1991).

Fig.11- Storm time variation of maximum electron density (N_mF2), in eight zones of geomagnetic latitude. The ordinate is the percentage deviation from quiet-day behavior (S. Matsushita, JGR, 64, 305, 1959).

Fig.12- Electron content, electron density and slab thickness at a mid-latitude station during an F region storm. SC marks the time of the sudden commencement. The 7-day means is also shown to indicate the normal behavior (Mendillo and Klobuchar, Report AFGRL-TR-74-0065, US Air Force, 1974).

Fig. 13- Diurnal characteristics of the F region density for the period September 14-29 1989, as measured by the critical frequency foF2 ($=8.9\ (10)^3\ N_mF2^{1/2}$ -(N_mF2 being in cm^{-3})- in a chain of northern midlatitude to high latitude stations. (Szuszczewicz et al., JGR, 103, 11,665-11,684, 1998).

Fig.14- The Auroral Activity index AE, the 3-hourly Planetary index K_p and the D_{st} values during 20-24 October 1989 corresponding the magnetic storm disturbance that had onset at ~08 UT on 20 October, plotted in the first top three panels. The two bottom panels show the variations of f_0F_2 and h_mF_2 during these days for the four locations Fortaleza (FZ), Cachoeira Paulista (CP), Concepción (CON) and King George Island (KGI). Horizontal patches indicate night hours for each of the stations. Horizontal lines with identification numbers, 1, 2, 3 etc. along the h_mF_2 plot over CP indicate intervals when positive and negative disturbances in meridional winds occurred.

Fig.15- Mass plot of vertical drift pattern over Jicamarca radar. The large increase of the vertical drift on one of the nights is due to a disturbance eastward electric field.

Fig.16- Variation pattern in response to the magnetic storm of 24-25 March in panels top to bottom (a) F layer height and peak density over Fortaleza, (b) same parameters over Cachoeira Paulista, (c) H- component of magnetic field, and (d) asymmetric ring current index which is equivalent to auroral activity index.

Fig.17- Variations in F layer heights over Fortaleza in Brazil and Hong Kong (top and middle panels). The disturbance has opposite polarity at the two location during the morning hours whereas the same polarity prevails in the evening hours.

Fig.18- Total electron content variation over Cachoeira Paulista during March 24-25 storm suggests poleward expansion of the equatorial anomaly peaks.

Fig.19- The variations of the F region height and peak density over the Brazilian stations Fortaleza and Cachoeira Paulista (located at the anomaly trough and crest, respectively) showing the large uplift of the layer in the dusk sector (to higher than the 1000 km limit

of the ionosonde), causing large TEC depletion confirming the anomaly peak dislocation suggested from Figs. 18,19 and 20.

Fig.20- TEC variations over Cachoeira Paulista in Brazil and over some higher latitude locations in Northern hemisphere during the great magnetic storm of March 1989, suggesting poleward expansion of the equatorial anomaly.

Fig.21- Contours of foF2 deviation vs. latitude and time for the Asian –Pacific sector during October 20-22, 1989

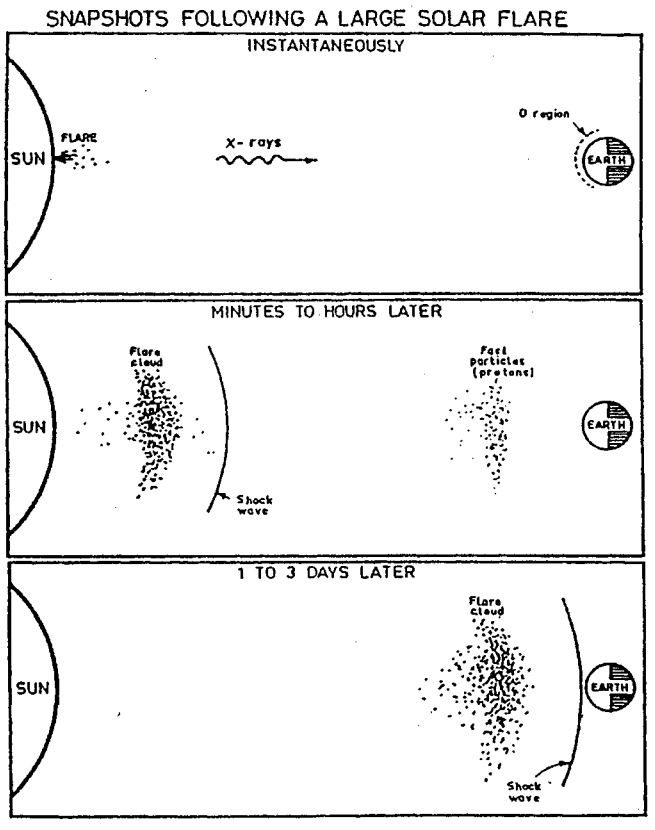

The three events in interplanetary space which follow a large solar flare :
(1.) Top. X rays are one form of radiation emitted by the flare. These travel in straight lines at the velocity of light, taking about 8 minutes to reach the Earth.
(2.) Middle. Fast protons reach the Earth after a delay which can be as short as a few minutes. These are followed by the more slowly moving flare cloud, which is preceded by a shock at the position where the clouds hits the quiet solar wind.
(3.) Lower. The flare cloud reaches the Earth a few days after being ejected from the flare.
Courtesy IPS Radio and Space Services.

Fig. 01

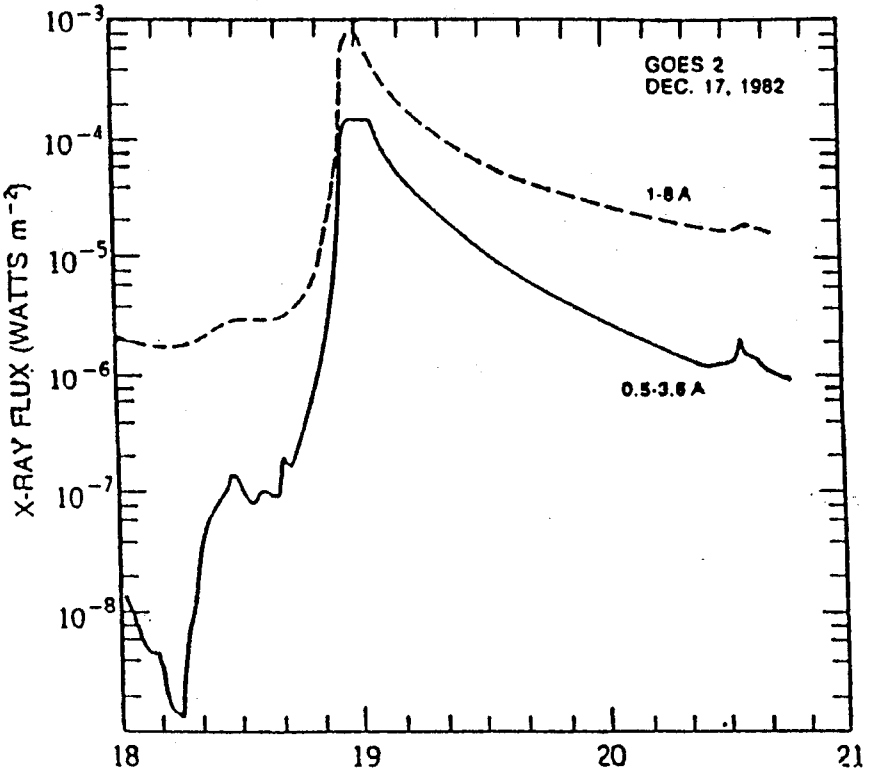

Sample X-ray flare showing sudden increase in the 1–8 Å and 0.5–3.6 Å channels. The hardness ratio (0.5–3.6 Å flux)/(1–8 Å flux) increases near the peak

Fig. 02

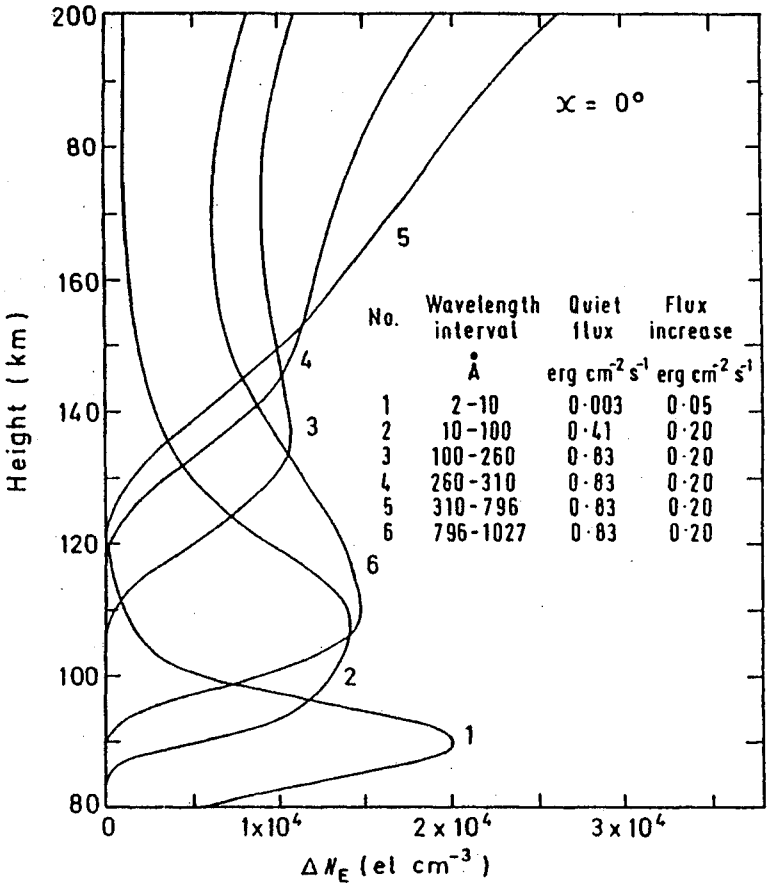

The computed increase of electron density due to flux increases in the stated wavelength intervals. (A. D. Richmond, private communication)

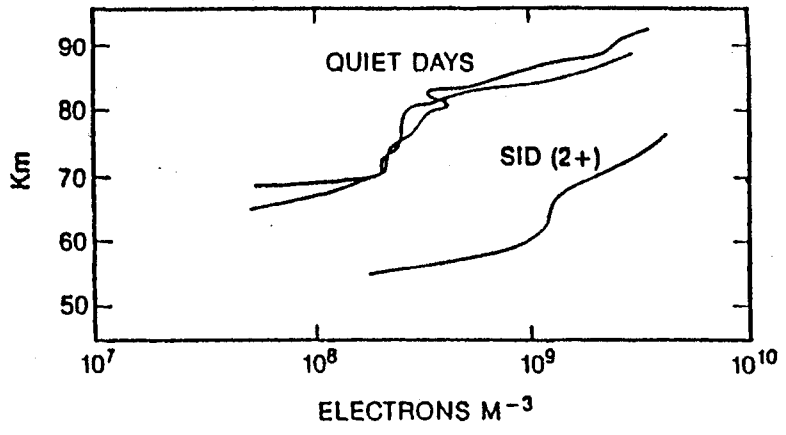

Electron-density profile on quiet days and during a 2+ flare, (After Be

Fig. 03

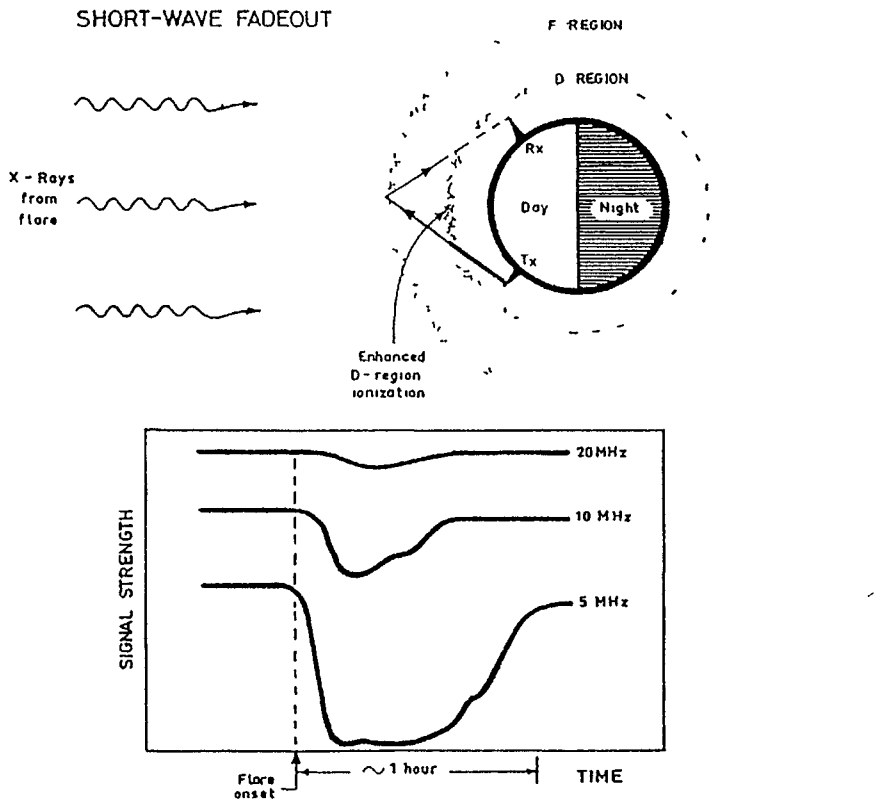

The effect of a short wave fade out (SWF) on the day-side ionosphere and on the signal strengths at frequencies of 5, 10, and 20 MHz on a circuit passing through the day side ionosphere X rays from the flare cause a large and sudden increase in the density of electrons in the D region, which causes a corresponding increase in the absorption suffered by an HF signal passing through it The low frequencies on an HF circuit are affected most and are the last to recover from the SWF The night-time side of the ionosphere is not affected by X rays *Courtesy IPS Radio and Space Services*

Fig 04a

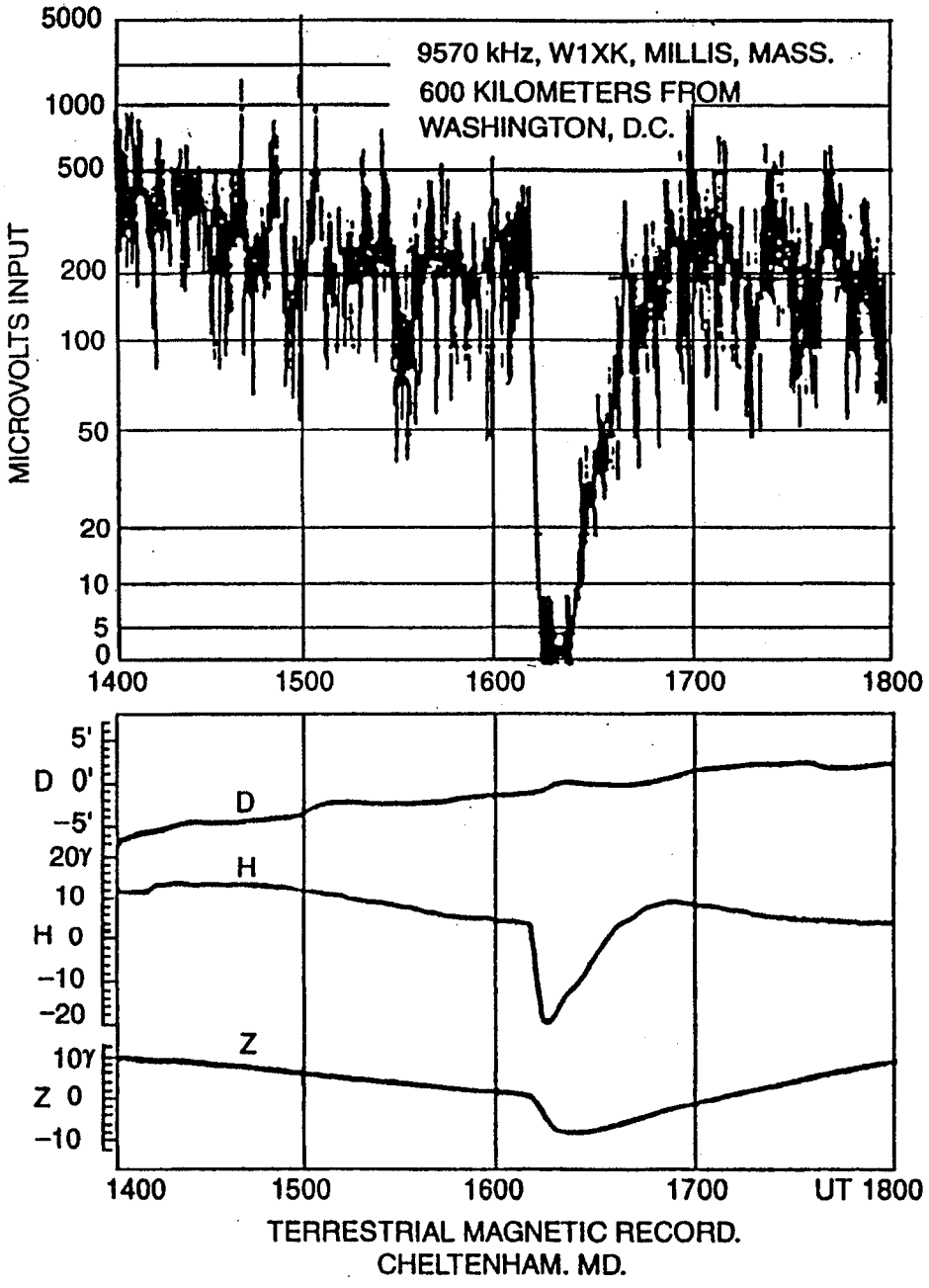

A short wave fadeout and a magnetic crochet (sudden flare effect) on November 26, 1936

Fig. 04b

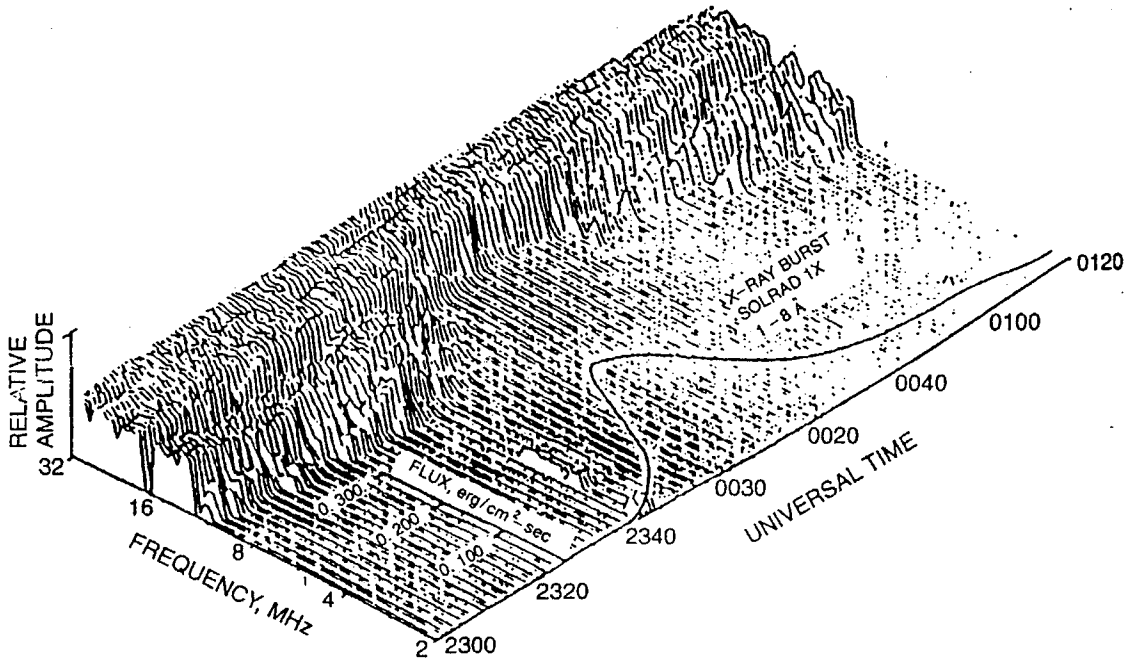

HF sounder data plot of an SWF variation with time of the radio frequencies observed on 30th October 1968 over the 4000 km path Hawaii to Corona, California during an X-ray burst. (Bleiweiss et al. 1973)

Fig. 05

Fig. 06

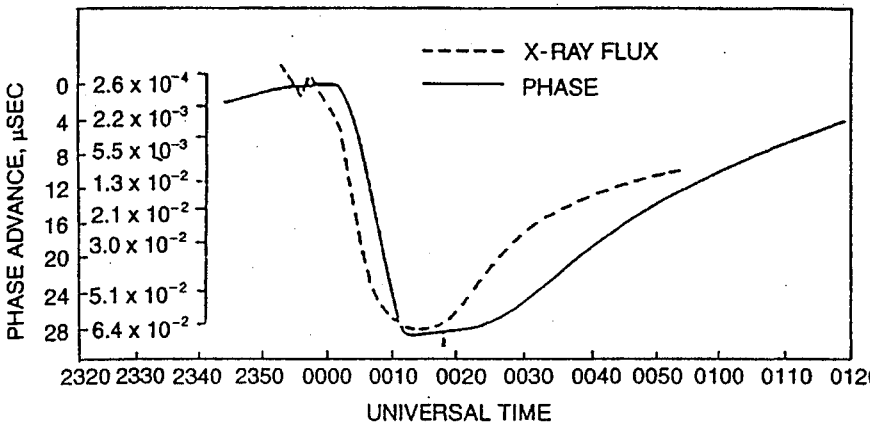

A comparison of the 9.34 kHz phase and the X-ray flux (inner scale, in ergs cm^{-2} s^{-1}) during a sudden phase anomaly on July 11–12, 1968. (Bleiweiss et al. 1973)

Fig. 07

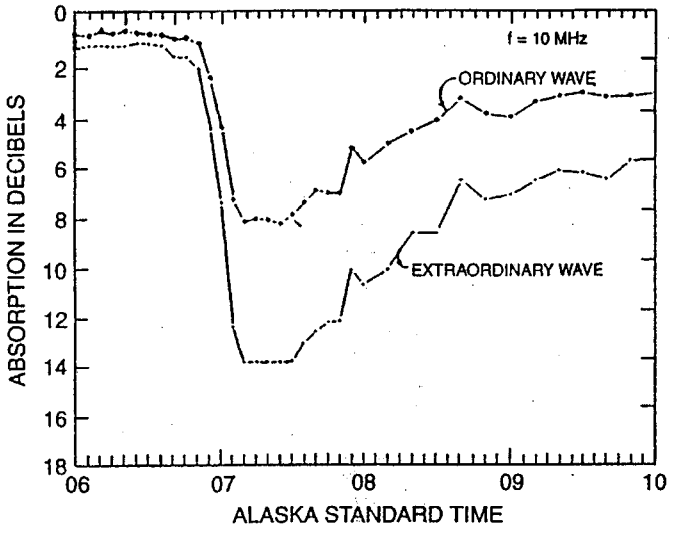

Sudden cosmic noise absorption, on 10 MHz, at College, Alaska June 11, 1961. (Lawrence et al. 1964)

Fig. 08

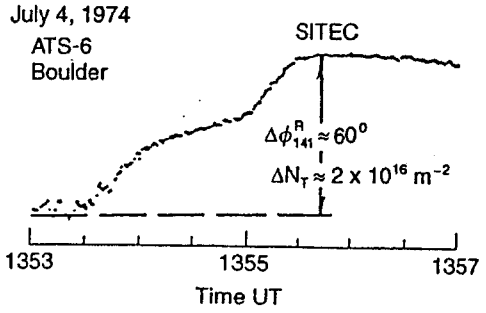

Sudden increase in total electron content, ATS6-Boulder, July 4, 1974

Fig. 06, 07, 08

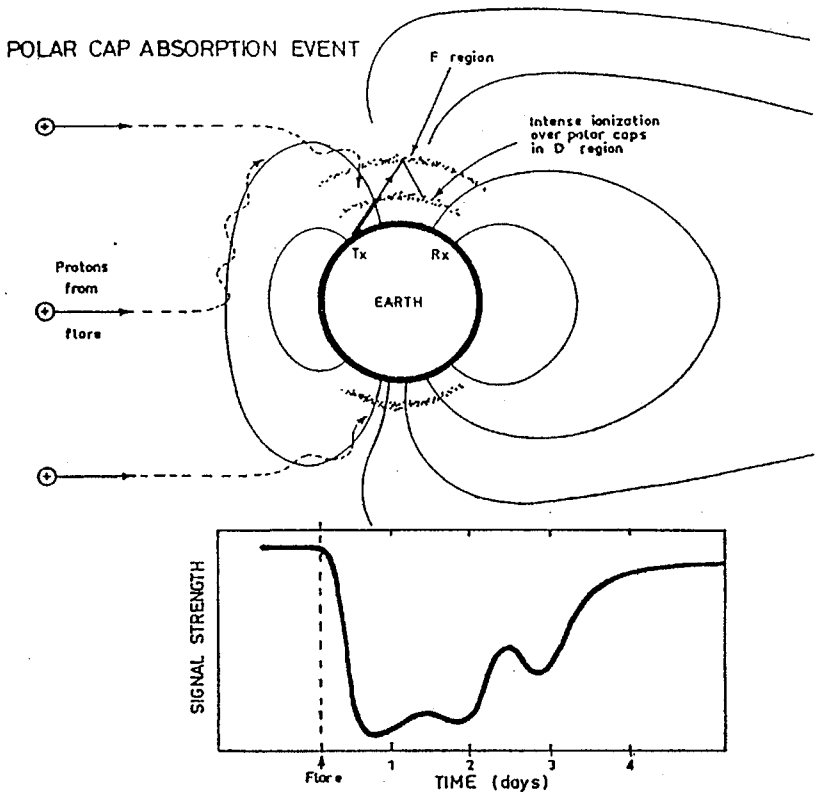

A polar cap absorption event (PCA) is caused by high-energy protons from large flares which penetrate to lower altitudes (the atmosphere over the polar regions of the Earth, thus causing large increases in the electron density in the polar D region. This increa in density leads to a large increase in HF absorption, which is known as a PCA. A PCA can last for days, depending on the output of proto from the flare. There is usually some recovery of the signal strength during the hours of darkness. *Courtesy IPS Radio and Space Service.*

Fig. 09

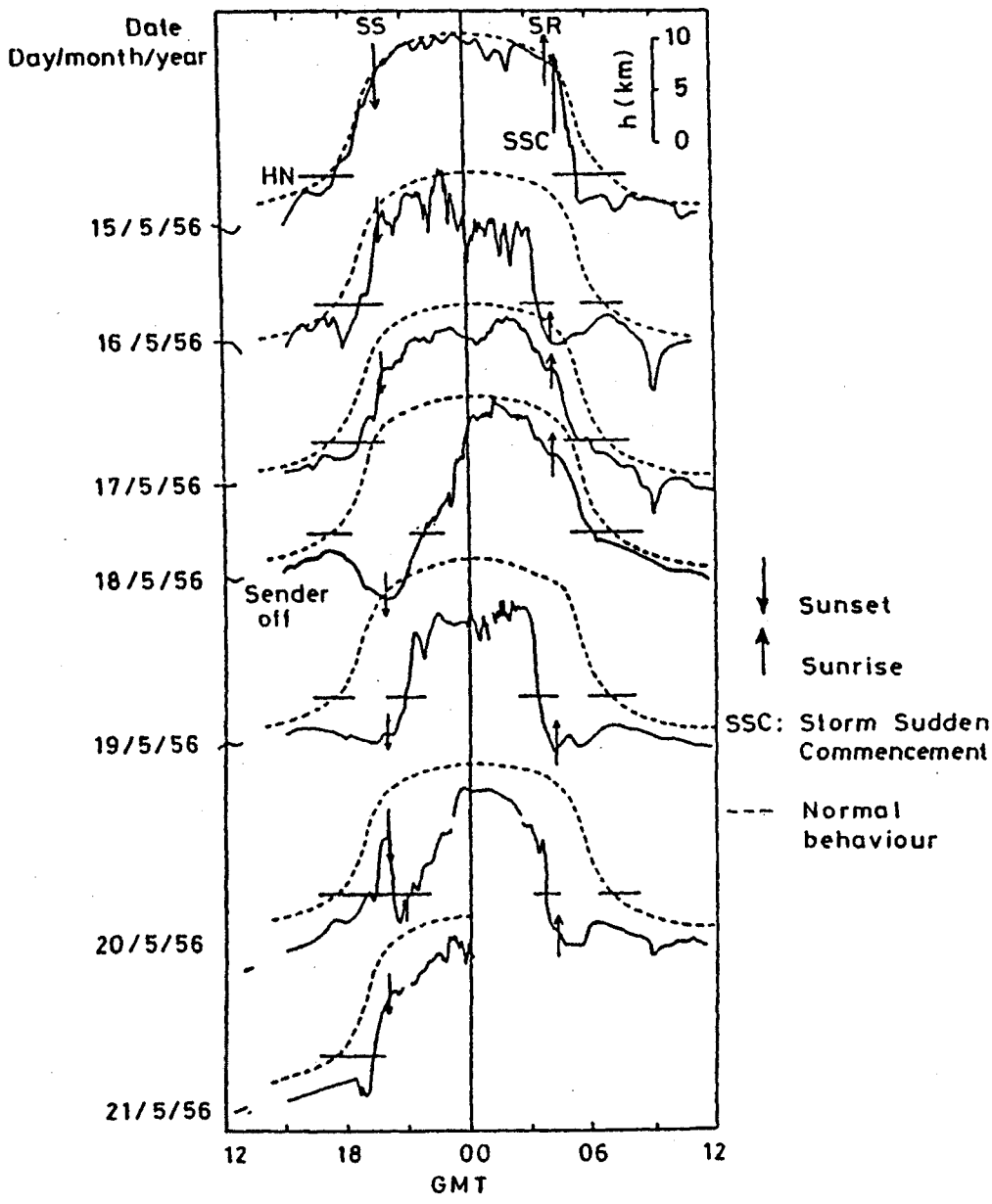

A D-region storm as seen in VLF radio propagation: reflection height of 16 kHz waves over the path Rugby–Cambridge, UK, during a magnetic storm in 1956. (J. S. Belrose, *AGARD Report* 29, 1968)

Fig. 10

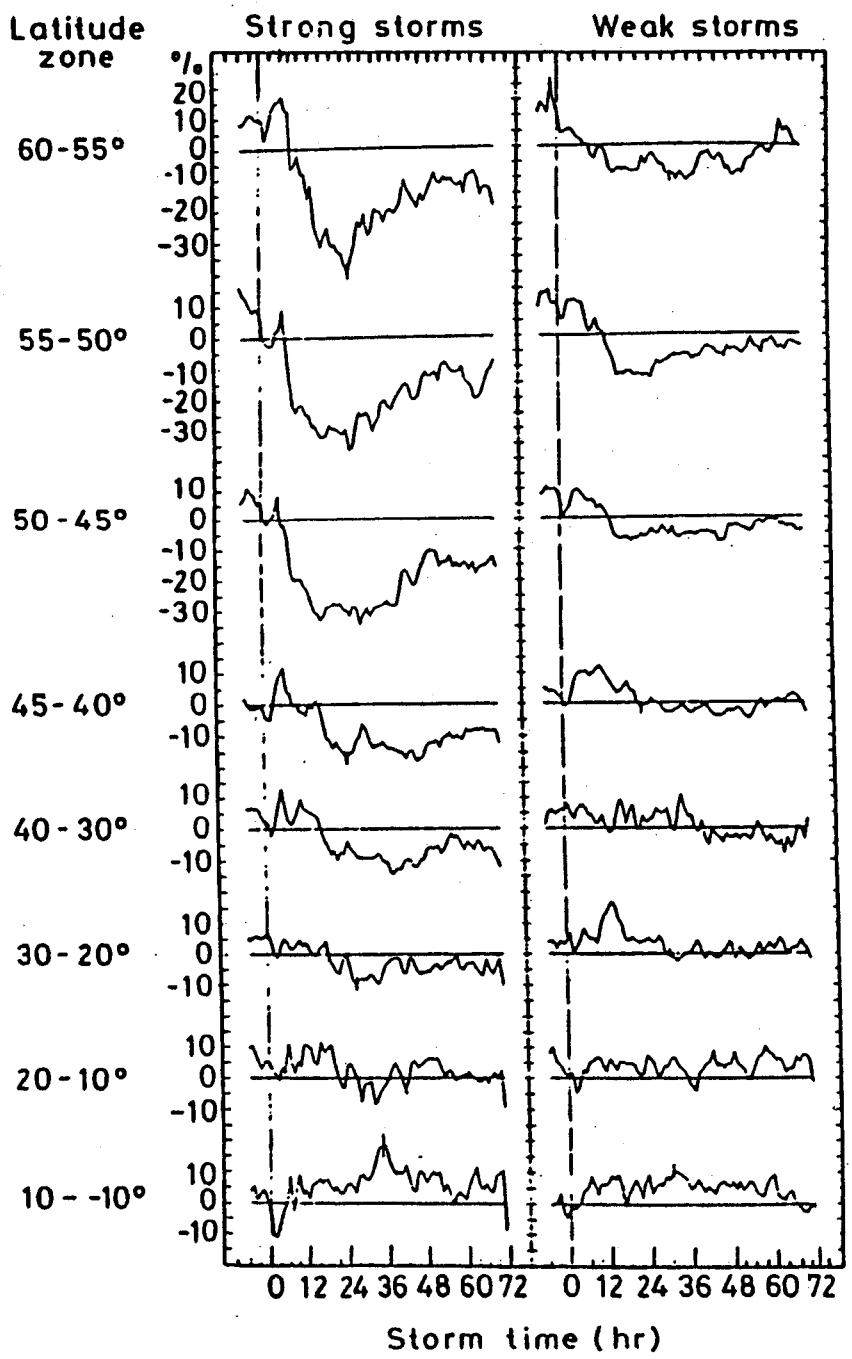

Storm-time (D_{st}) variations of maximum electron density (N_mF2), in eight zones of geomagnetic latitude. The ordinate is the percentage. deviation from quiet-day behaviour. (After S. Matsushita, *J. Geophys. Res.* **64**, 305, 1959, copyright by the American Geophysical Union)

Fig. 11

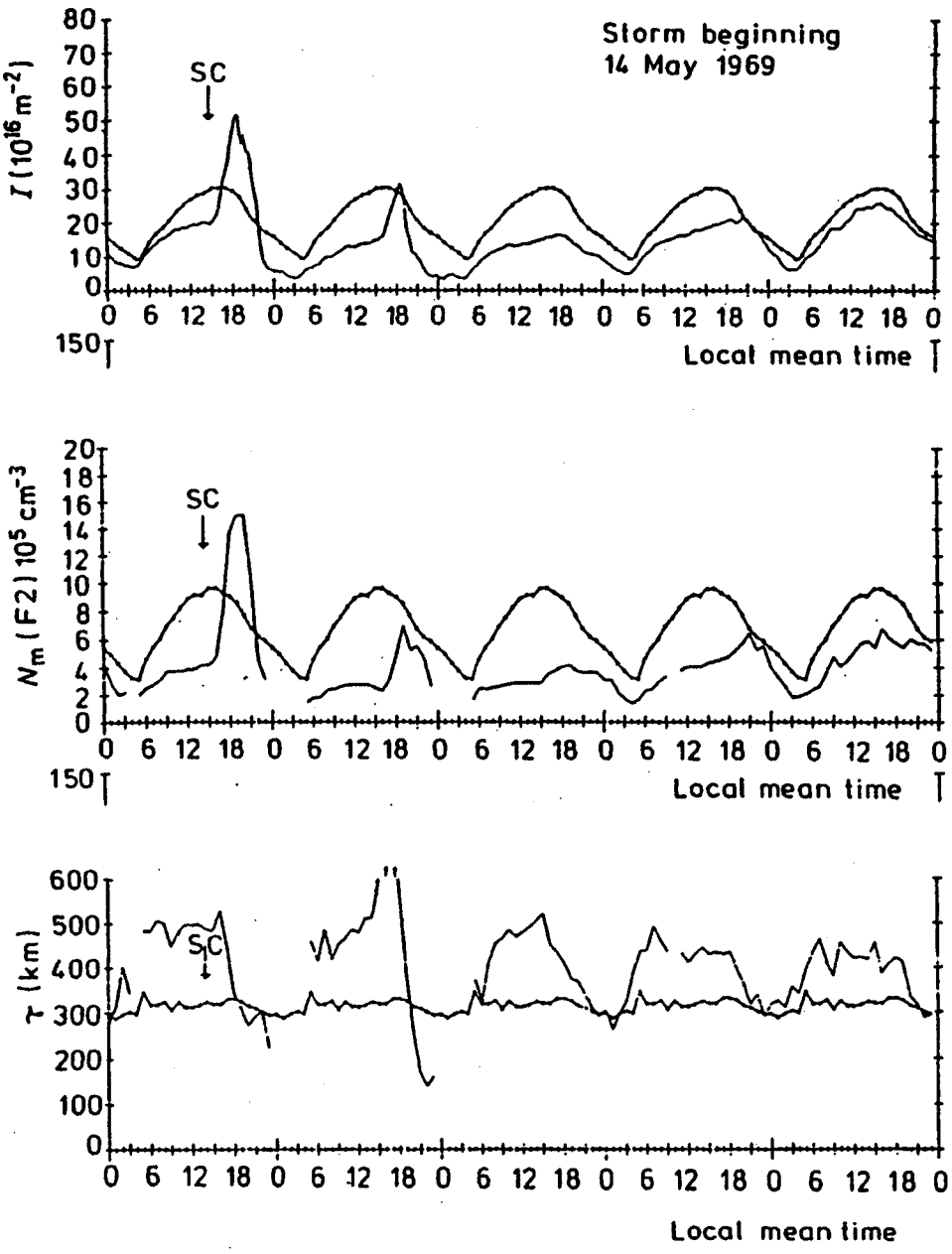

Electron content, electron density and slab thickness at a mid-latitude station during an F-region storm. SC marks the time of the sudden commencement. The 7-day mean is also shown to indicate normal behaviour. (M. Mendillo and J. A. Klobuchar, *Report AFGRL-TR*-74-0065, US Air Force, 1974)

Fig. 12

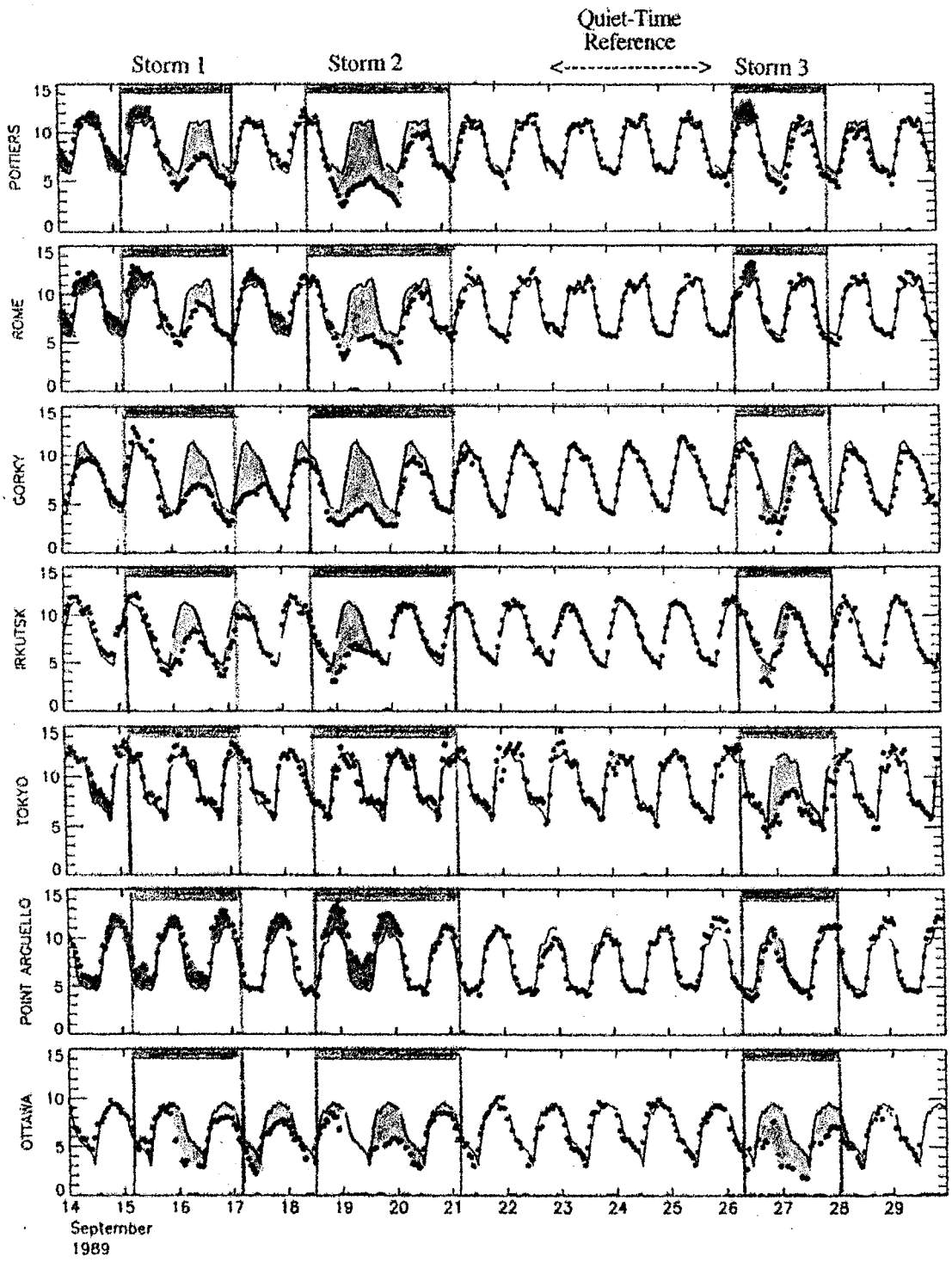

Diurnal characteristics of the F region density for the period September 14-29, 1989, as measured by the critical frequency $f_0F_2(=8.9(10)^3\{N_mF_2[cm^{-3}]\}^{1/2})$ in a longitudinal chain of northern mid-latitude to high latitude stations. Top to bottom: Poitier (0.3°E, 46.6°N), Rome (12.5°E, 41.8°N), Gorky (44.3E, 56.2°N), Irkutsk (104.0°E, 52.5°N), Tokyo (139.5°E, 35.7°N), Point Arguello (239.4°E, 35.6°N), and Ottawa (284.1°E, 45.4°N).

Fig. 13

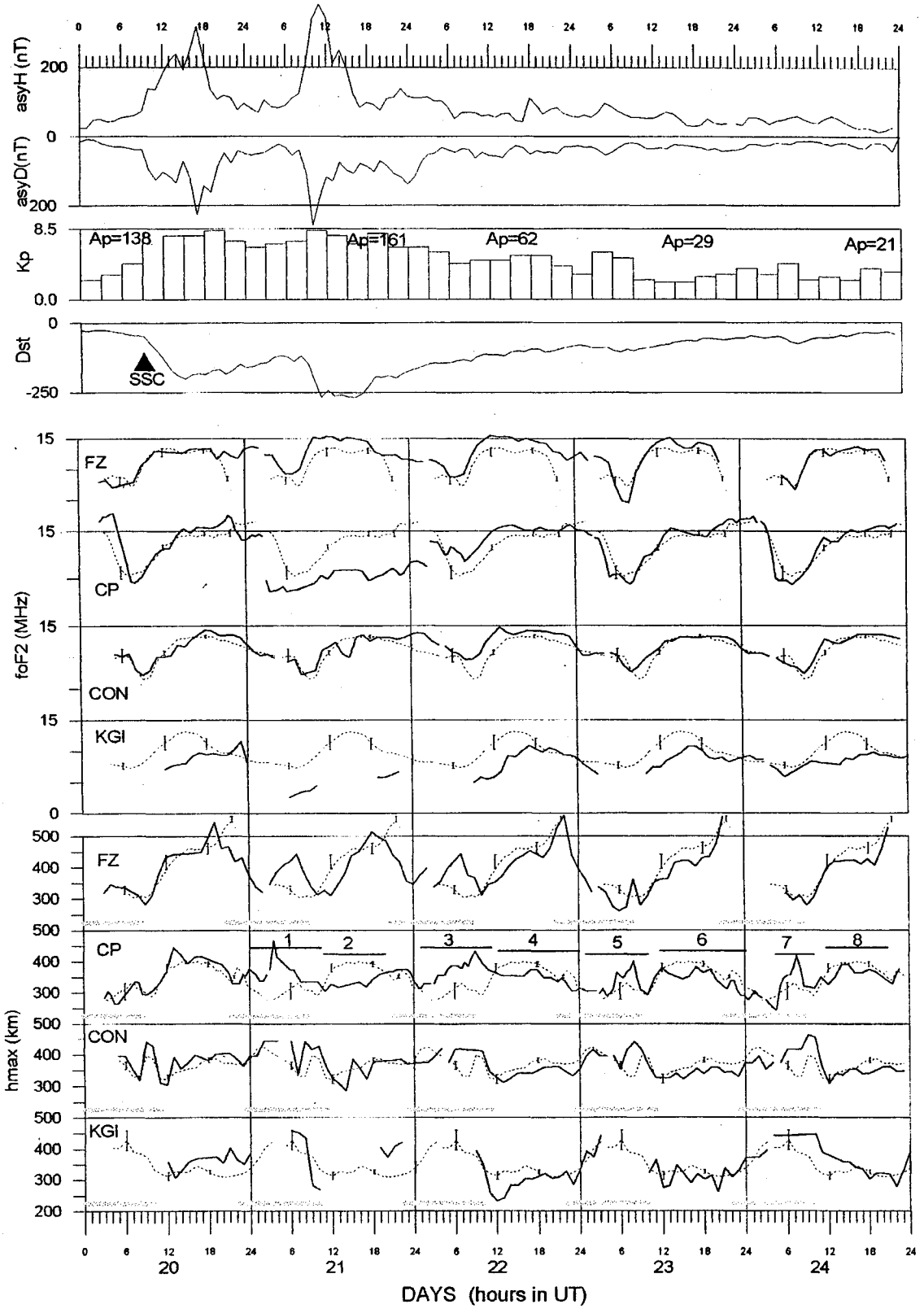
asyH (nT)
200
0
asyD(nT)
-200
Kp
8.5
0.0
Ap=138
Ap=161
Ap=62
Ap=29
Ap=21
Dst
0
-250
SSC
foF2 (MHz)
FZ
CP
CON
KGI
hmax (km)
500
400
300
200
1
2
3
4
5
6
7
8
0
6
12
18
24
20
21
22
23
24
DAYS (hours in UT)

Fig. 14

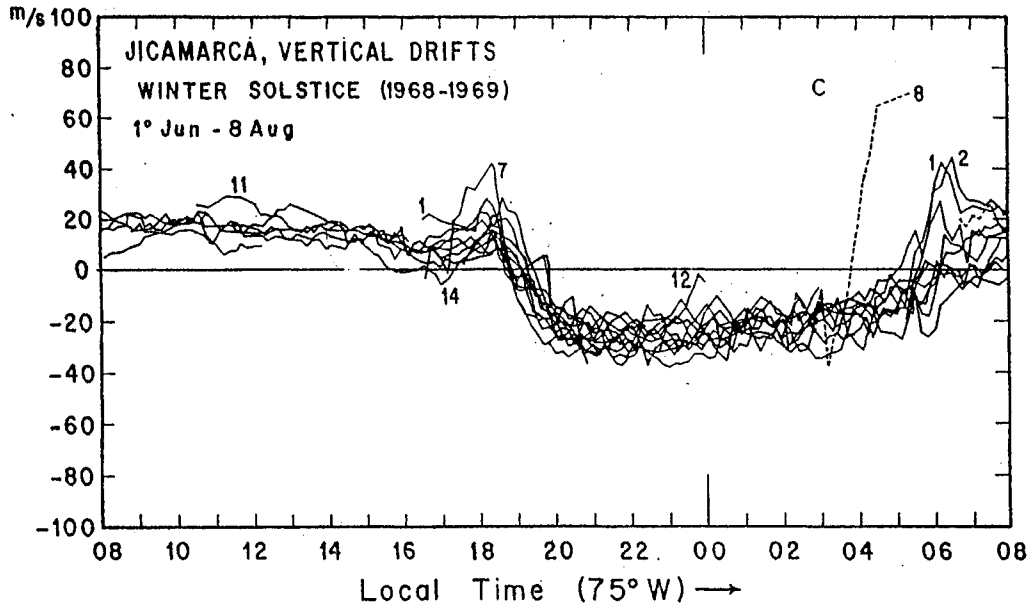
m/s 100
80
60
40
20
0
-20
-40
-60
-80
-100
JICAMARCA, VERTICAL DRIFTS
WINTER SOLSTICE (1968-1969)
1° Jun - 8 Aug
C
8
11
7
1
14
12
1
2
08
10
12
14
16
18
20
22
00
02
04
06
08
Local Time (75° W) ⟶

Fig. 15

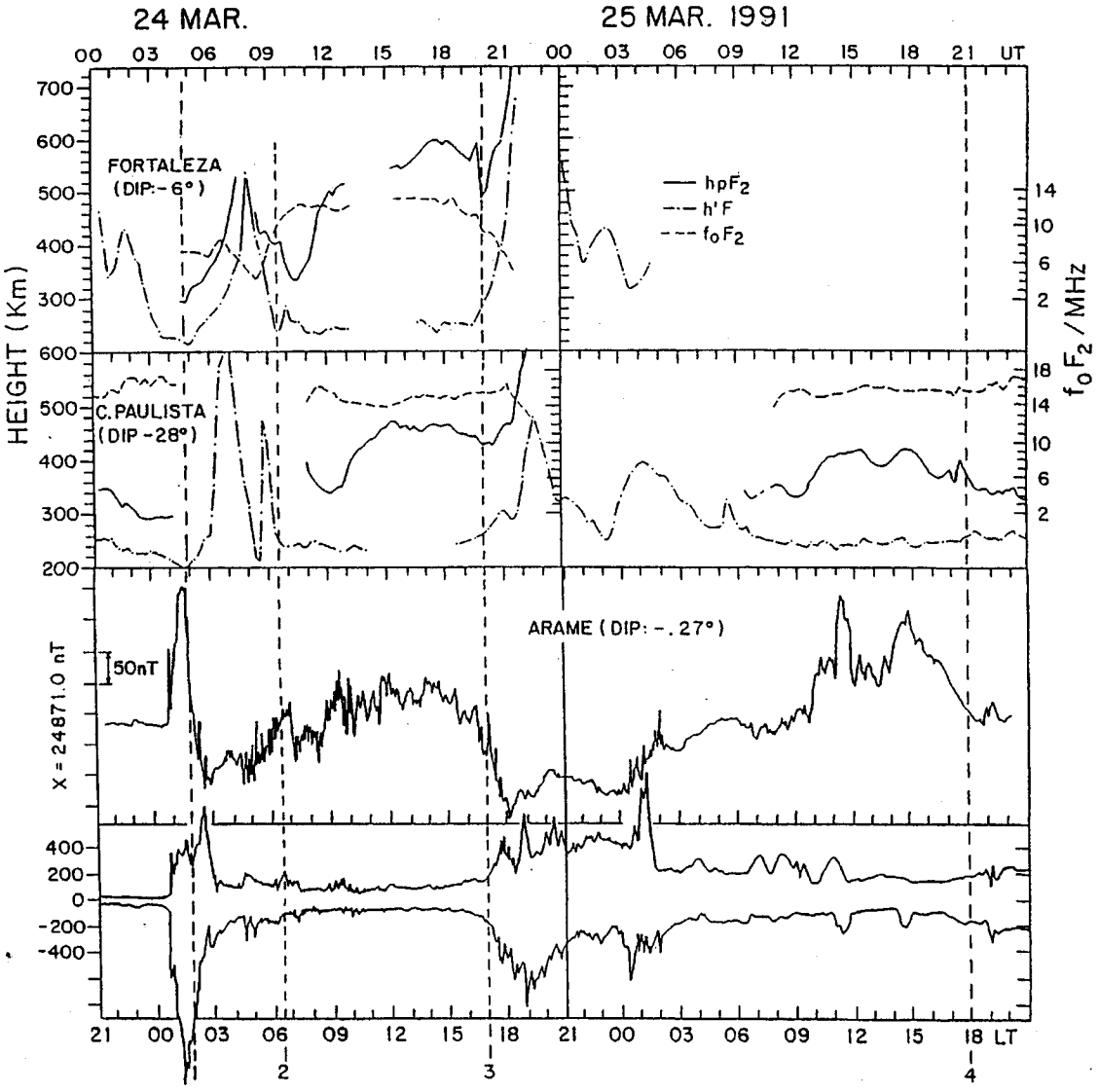

Variations during the magnetic storm of 24–25 March 1991 in: (a) The F-layer height parameter $h'F$ and h_pF_2 and the peak density represented by f_0F_2 over Fortaleza. (b) The same parameter as in (a), for Cachoeira Paulista. (c) H component from the magnetogram over Arame, Brazil. (d) Asymmetric ring current indices in H and D components represented by ASY-H and ASY-D (Iyemore *et al.*, 1993).

Fig. 16

Ionospheric electric field variations with local time and longitude

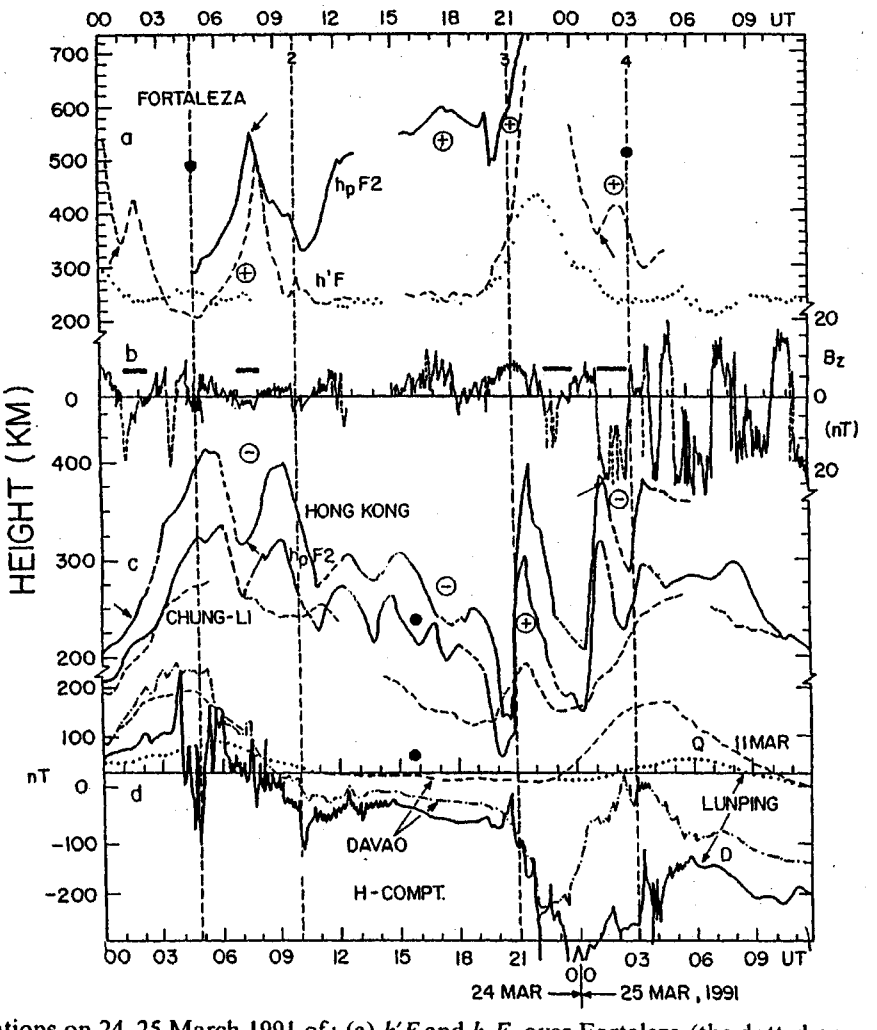

Variations on 24–25 March 1991 of: (a) $h'F$ and h_pF_2 over Fortaleza (the dotted curve is the quiet day $h'F$ variation); (b) IMF B_z component from the IMP-8 satellite; (c) h_pF_2 over Hong Kong and Chung-Li (the dashed curve represents the quiet day variation of h_pF_2 over Chung-Li); (d) Magnetic field H components over Davao and Lunping (Q, for quiet days, the dashed and dotted curves; and D for disturbed days, the dashdotted and solid curves). The circled + and − signs in a and c indicate positive and negative polarities of the disturbance electric fields suggested in the respective height variation features.

Fig. 17

Ionospheric electric field variations with local time and longitude

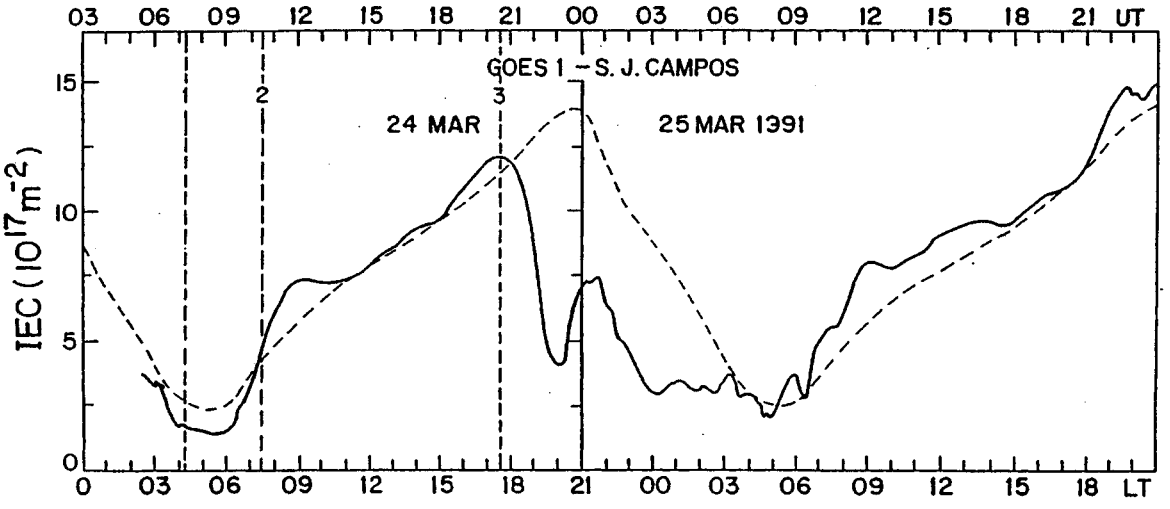

Ionospheric Electron Content (IEC) measured at Cachoeira Paulista from Faraday rotation of the 136MHz beacon signal from the Geostationary Satellite GOES-I, during 24–25 March 1991. Note the morning minor depletion in IEC at predawn hours around the vertical line 1 followed by an enhancement around line 2, and a large depletion in IEC indicating a major expansion of the EIA poleward of C. Paulista, starting at ~1730 LT (vertical line 3).

Fig. 18

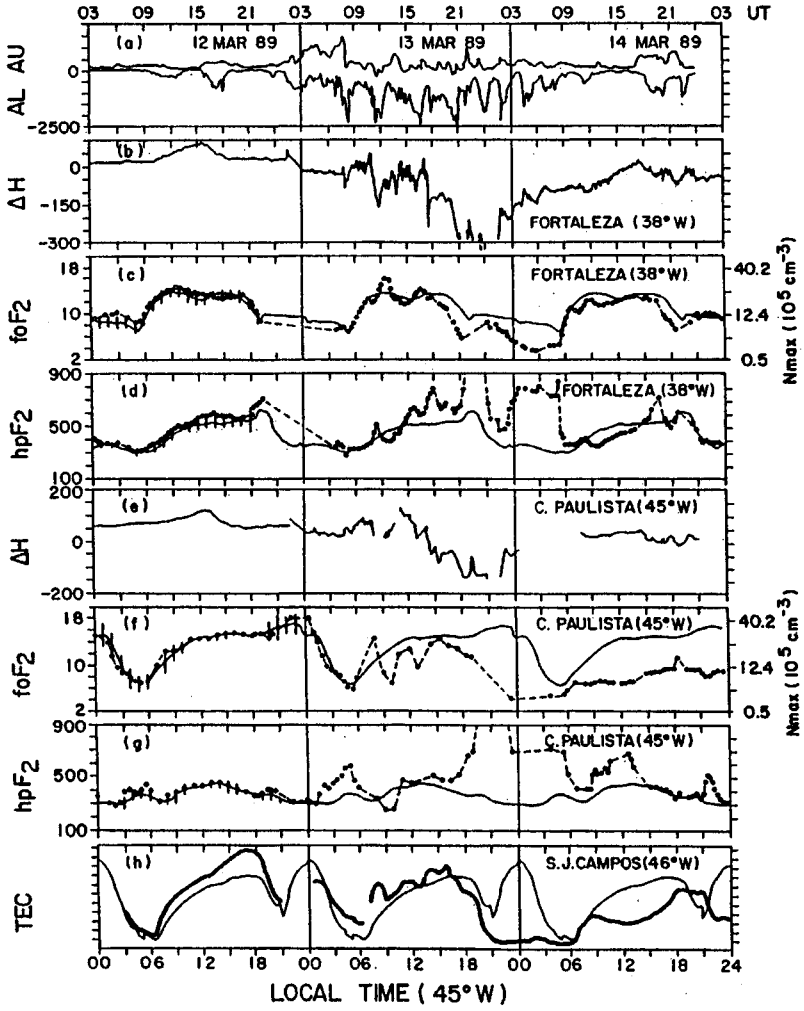

(a) Auroral electrojet indices. *(b)* Horizontal component of the magnetic field in Fortaleza, in gammas. *(c)* and *(d)* $foF2$ (in megahertz) and $hpF2$ (in kilometers) over Fortaleza for the period March 12-14, 1989 (open circles), and quiet time reference curve (thin line). *(e)* Horizontal component of the magnetic field at Cachoeira Paulista, in gammas. *(f)* and *(g)* $foF2$ (in megahertz) and $hpF2$ (in kilometers) over Cachoeira Paulista. *(h)* Relative changes in total electron content over São José dos Campos for the period March 12-14, 1989 (thick line), and quiet time mean (thin line). Each division on the vertical axis of TEC is equal to a variation of 1.1×10^{17} el m^{-2} in TEC (or 180° in Faraday rotation angle).

Fig. 19

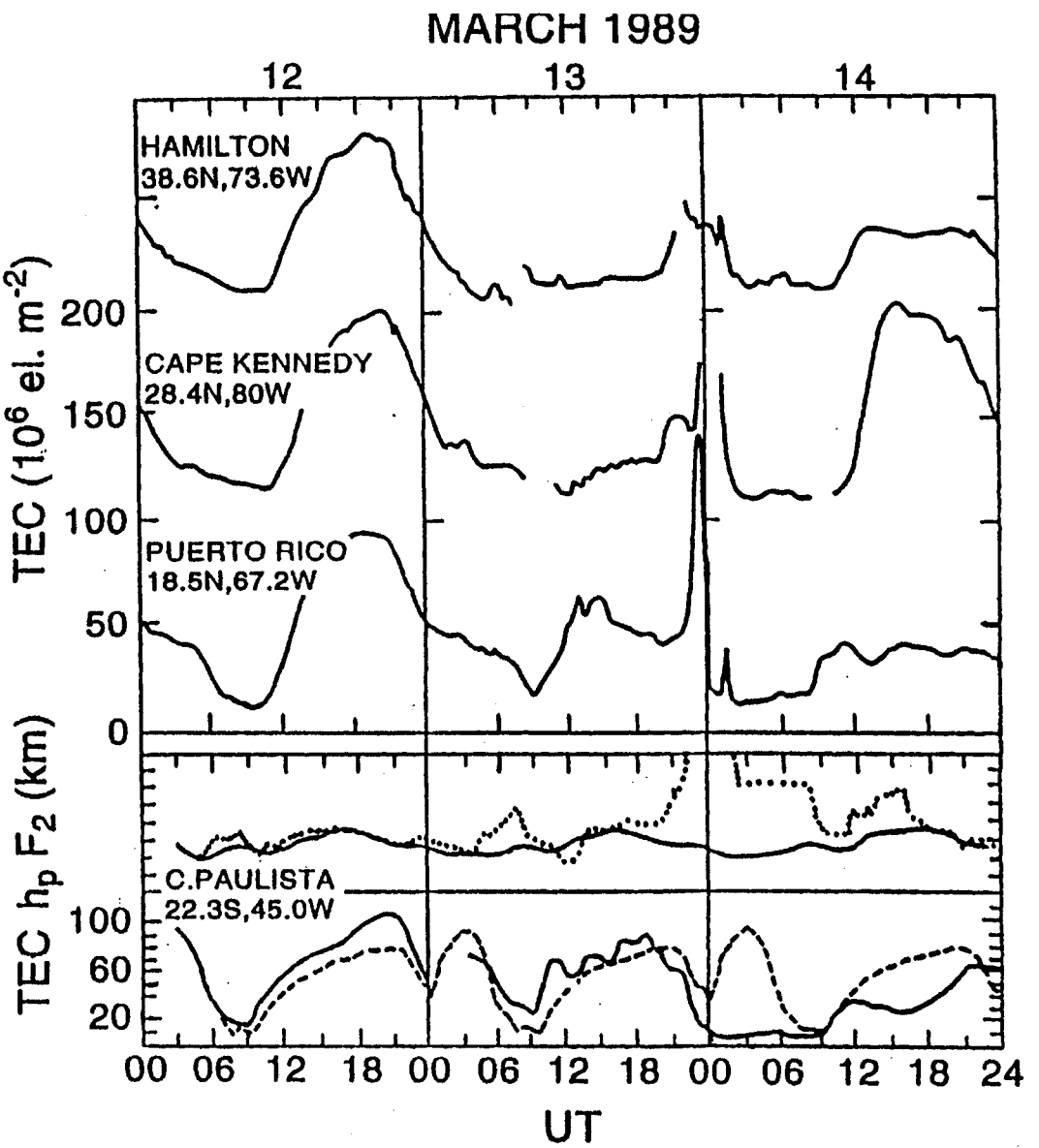

TEC (Total Ionospheric Electron Content) observed during the great storm of 13 March 1989, from bottom upward: over Cachoeira Paulista, Puerto Rico, Cape Kennedy and Hamilton. The *hpF*2 values for Cachoeira Paulista are shown (with solid line representing the reference quiet day curve) in the bottom panel. The TEC quiet day reference is shown by,the dashed line.

Fig. 20

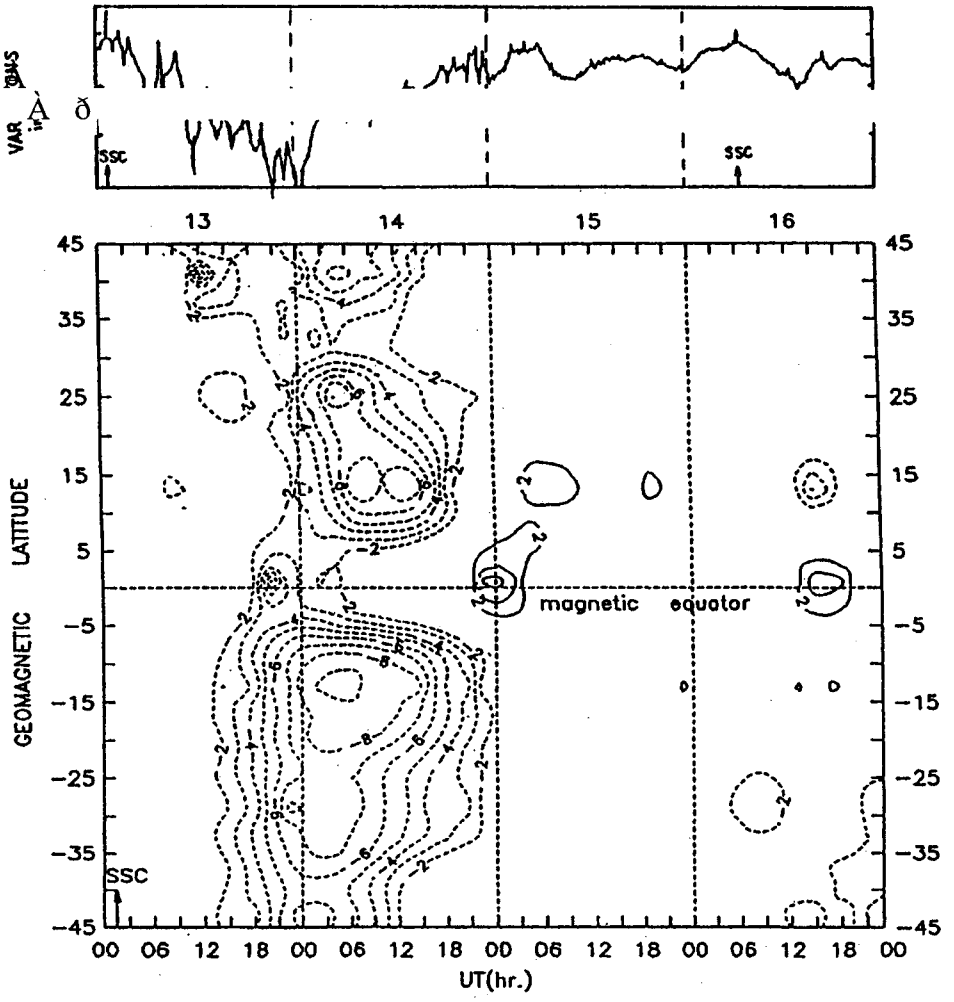

Contours of foF2 deviations versus time and latitude for the Asian/Pacific sector during 13–16 March 1989. Diurnal foF2 on 12 March is used as a quiet time reference. The solid line indicates a positive deviation, corresponding to positive storm effects and the dashed line indicates a negative deviation, corresponding to negative storm effects. The interval between adjacent contours is 1.0 MHz. The deviations in foF2 can be interpreted in terms of those in electron density by noting that a change of 2, 4, or 8 MHz in foF2 at 10 MHz corresponds nearly to an electron density change of 5, 10 or 20 $\times 10^{11}$ el./m^3, respectively. The top panel shows the H-component of the geomagnetic field recorded at Lunping Observatory (replotted from Huang and Cheng, 1991), and each division corresponds to an increment of 200 nT.

Fig. 21